Article:
Migliorini, E, Horn, P, Haraszti, T et al. (5 more authors) (2017) Enhanced Biological Activity of BMP-2 Bound to Surface-Grafted Heparan Sulfate. Advanced Biosystems, 1 (4). ARTN 1600041. ISSN 2366-7478

https://doi.org/10.1002/adbi.201600041

DOI: 10.1002/((please add manuscript number))
Article type: Communication

Title: Enhanced biological activity of BMP-2 bound to surface-grafted heparan sulfate

Elisa Migliorini, Patrick Horn, Tamás Haraszti, Seraphine V. Wegner, Christian Hiepen, Petra Knaus, Ralf P. Richter and E. Ada Cavalcanti-Adam**

Dr. E. Migliorini, Dr. S. V. Wegner, Prof. E.A. Cavalcanti-Adam
Department of Biophysical Chemistry, Institute of Physical Chemistry, Heidelberg University, Im Neuenheimer Feld 253, 69120 Heidelberg, Germany
Department of Cellular Biophysics, Max Planck Institute for Medical Research, Postal Address: Heisenbergstr. 3 D-70569 Stuttgart, Germany
E-Mail: migliorini@is.mpg.de; ada.cavalcanti-adam@urz.uni-heidelberg.de
Dr. P. Horn
Department of Medicine V, Heidelberg University, INF 410, 69120 Heidelberg, Germany
Dr. T. Haraszti
DWI - Leibniz Institute for Interactive Materials, Forkenbeckstr. 50 52056 Aachen, Germany
Dr. S.V. Wegner
Department of Biophysical Chemistry, Institute of Physical Chemistry, Heidelberg University, Im Neuenheimer Feld 253, 69120 Heidelberg, Germany
Max Planck Institute for Polymer Research, Ackermannweg 10, 55128 Mainz, Germany
Dr. C. Hiepen, Prof. P. Knaus
Institute of Biochemistry, Freie Universität Berlin, Thielallee 63, 14195 Berlin, Germany
Dr. R. P. Richter
University of Leeds, School of Biomedical Sciences and School of Physics and Astronomy, Leeds, LS2 9JT, UK; CIC biomaGUNE, Biosurfaces Lab, Paseo Miramon 182, 20009 San Sebastian, Spain; University Grenoble-Alpes and CNRS, Laboratory of Interdisciplinary Physics, 140 Rue de la Physique, 38402 St. Martin d'Hères, France

Keywords: BMP-2, heparan sulfate, extracellular matrix, noggin, biomimetic platforms

Bone morphogenetic protein-2 (BMP-2) is known to initiate the differentiation of mesenchymal stem cells (MSCs) into osteoblasts and chondrocytes *in vivo* and *in vitro*,[1] as well as the transdifferentiation of mouse myoblasts C2C12 cell line into mineralizing bone-like cells.[2, 3] The BMP-2 signaling pathway is activated by the binding of the growth factor to two types of transmembrane serine/threonine kinase receptors, the BMP type I (BMPRI) and type II (BMPRII) receptors. Binding of BMP-2 to BMPRI and BMPRII induces the phosphorylation of the SMAD1/5/8 complex, which then together with co-SMAD (SMAD4) translocates to the nucleus and, with other DNA-binding proteins, participates in the transcriptional regulation of osteogenic target genes.[4]

The clinical use of BMP-2 was approved in 2002 by the Food and Drug Administration in the USA and validated by the national Medical Agencies in Europe. BMP-2 has been rapidly introduced into orthopedic clinical practice[5] but, in some cases, even high doses (up to 2 mg/level) appear only marginally effective, likely due to an autocrine BMP-2 inhibition by noggin the major extracellular BMP antagonist, at sites of BMP-2 application.[6] Therefore, improving BMP-2 activity, by using delivery systems that suppress BMP-2 inhibition by noggin, would help in overcoming current challenges in BMP-2 clinical application.[7]

The development of materials that are able to control BMP-2 molecular presentation and local concentration, is an essential approach for a deeper understanding of BMP-2 functions and the modulation of its biological activity.[8]

In tissues, BMP-2 is bound to extracellular matrix (ECM) components such as proteins[9] and glycosaminoglycans (GAGs), in particular to heparan sulfate (HS)[10, 11]. BMP-2 is a homodimeric protein and has been reported to bind *in vitro* to heparin (Hp), a highly sulfated form of HS, *via* a binding site located at the N-terminus (**Figure 1A**) with an affinity of approximately 20 nM.[12] The binding of BMP-2 to HS, on the other hand, remains to be fully characterized in terms of stoichiometry, affinity and concomitant HS morphological changes. HS, a linear polysaccharide formed by variably sulfated repeating disaccharide units, is typically covalently attached to core-proteins forming HS proteoglycans (HSPGs). The functions of HSPGs depend on their structure and location, being either at the cell surface or as part of the ECM.[13]

Contradictory effects of cell surface HSPGs on BMP-2 activity have been reported. On the one hand, endogenous HSPGs negatively modulate both chondrogenic[14] and osteogenic[10] differentiation by inhibiting the activation of BMP-2 signaling. On the other hand, HSPGs act as BMP-2 co-receptors, promoting the formation of complexes between BMPRII and BMPRI, thereby enhancing the bioactivity of BMP-2.[15] Interestingly, the BMP antagonist noggin also binds to HS.[16] Once bound to cell surface HSPGs, noggin maintains its function to inhibit

the activity of BMP-4, another member of the BMP family, by blocking the binding epitopes for BMPRI and BMPRII.[16, 17]

To date, the role of HSPGs in the extracellular space (ECM-HSPGs) on BMP-2 bioactivity is only partially explored. The main functions so far attributed to ECM-HSPGs are to prevent the diffusion of growth factors away from the regions where they are likely to be required.[18] However, it is still unknown if these HSPGs can positively modulate BMP-2 biological activity thus enhancing *in vitro* osteogenic differentiation.[19]

The presence of HS added to the culture media of BMP-responsive cells (C2C12 myoblasts) prolongs SMAD 1/5/8 phosphorylation in these cells and reduces the interactions with the antagonist noggin,[11, 20] in contrast to the effect of cell surface HSPGs.[16] Since *in vivo* HS is not in solution, but rather covalently bound to core-proteins through its reducing end forming HSPGs,[21] administering HS in the cell culture media is unlikely to be representative of the *in vivo* extracellular HS.

Biomimetic platforms presenting HS in a bound and oriented manner are therefore suitable to explore (i) the characteristics of HS/BMP-2 binding at the molecular and cellular levels, (ii) the impact of BMP-2 presentation on BMP-2 activity, and (iii) the interaction of noggin with grafted HS and its recognition of the HS-bound BMP-2. The strength of such platforms lies in the precise molecular presentation, which gives the ability to control and characterize BMP-2 interactions with HS, as well as the possibility to further exploit them as substrates for investigations on the impact of HS on BMP-2 activity in cells. We designed our model surfaces in a way that HS is grafted by its reducing end,[22] mimicking its attachment to HSPG core proteins *in vivo*. To this end, we functionalized the reducing end of HS with biotin and used gold-coated surfaces functionalized first with a mixed monolayer of oligoethyleneglycol (OEG)-thiol and biotin-OEG-thiol and then with a streptavidin monolayer as substrates[23] (**Figure 1B**). The OEG monolayer passivates against non-specific binding of proteins, here tested using bovine serum albumin (BSA) (**Figure S1**), whereas streptavidin (SAv) binds

through a specific interaction with the biotin end-groups and forms a rigid monolayer. Such monolayer serves then as a mediator for the immobilization of biotinylated compounds such as biotinylated HS (b-HS; **Figure 1C**) and biotinylated BMP-2 (b-BMP2; **Figure 1D**). BMP-2 binds to SAv *via* a biotin-PEG_{12}-NHS ester linker (of ~5.6 nm contour length) which reacts with primary amines of the growth factor. Surface functionalization steps, specificity of the molecular binding and mechanical properties of the biomolecular films were characterized by quartz crystal microbalance with dissipation monitoring (QCM-D); adsorption and desorption rates of the different biomolecules, as well as biomolecular surface densities, were quantified by spectroscopic ellipsometry (SE).

Figure 1C and **D** shows QCM-D characterization of the two biomimetic platforms (Δf and ΔD correspond to the fifth overtone). After the formation of a SAv monolayer with an expected thickness of approximately 4 nm [24] (determined using Sauerbrey's equation; **Figure 1C**, 60 to 80 min), b-HS adsorbs rapidly forming a hydrated and soft film, indicated by the increase in dissipation of $4.5 \pm 0.5 \times 10^{-6}$ (**Figure 1C**, 90 to 110 min). BMP-2, incubated at a concentration of 96 nM, stably binds to the b-HS film causing an increase in film rigidity, as demonstrated by the negative dissipation shift of $-0.9 \pm 0.1 \times 10^{-6}$ (**Figure 1C**, 150 to 180 min). Complementary assays based on fluorescence recovery after photobleaching (FRAP), using films of b-HS grafted to supported lipid bilayers in the fluid phase, revealed that BMP-2 binding reduces the lateral mobility of HS chains substantially. This suggests that the increased rigidity arises from cross-linking of HS chains mediated by the growth factor (**Figure S2)**. This phenomenon has been reported for other ECM signaling proteins, such as chemokines and growth factors, some of which present multiple HS binding sites.[26] We speculate that HS cross-linking induced by BMP-2 might be due to the presence of two or more independent Hp/HS binding sites at the N-terminus region of the BMP-2 dimer, as previously predicted.[25] A mutant form of BMP-2, EHBMP-2, where the N-terminal region responsible for the Hp binding was substituted by a heterologous sequence from human

interleukin-2,[12] does not bind to b-HS (**Figure 1C**, grey curve) and does not induce HS film cross-linking (**Figure S2)**. This demonstrates that BMP-2 binds HS specifically through the same site as Hp.

For comparison, we also adopted a second BMP-2 immobilization strategy that does not involve HS. In this case, biotinylated BMP-2 (b-BMP2) binds directly to the SAv monolayer until saturation (**Figure 1D**, 50 to 110 min). When incubated at the same concentration (96 nM) without the biotin tag, BMP-2 does not bind stably (**Figure 1D**, gray curve) demonstrating the b-BMP2 is specifically attached *via* biotin to the SAv monolayer.

To quantify the binding strength of BMP-2 to b-HS films, we used spectroscopic ellipsometry (SE) and performed a titration assay (**Figure S3A**). The titration curve (**Figure S3B**) was approximated well by the simple Langmuir isotherm:

$$\Gamma_{eq} = \Gamma_{max} \frac{[BMP-2]}{K_d + [BMP-2]}, \quad (1)$$

with an affinity of $K_d \approx 1.6$ μM and a maximal BMP-2 surface density of $\Gamma_{max} \approx 1000$ ng/cm^2. For this analysis, it has to be considered that HS is not a homogeneous polymer: the constituent monosaccharides are variably sulfated and/or might exist as different epimers, (regions of high sulfation coexisting with regions of low sulfation along individual HS chains). These structural features can also vary from one HS source to another.[27, 28] It is therefore likely that HS presents a spectrum of binding sites rather than a single type. The affinity constant of 1.6 μM should thus be considered as an effective value, resulting from a spectrum of binding sites with different affinities.[29] For comparison, an affinity of 20 nM for Hp has been previously reported,[12] indicating that a high degree of sulfation might indeed substantially enhance the effective binding strength in comparison to the value obtained here. At the maximal surface density predicted by the Langmuir isotherm (Γ_{max} = 1000 ng/cm^2), we calculated that up to 11 BMP-2 dimers would bind to a 12 kDa b-HS chain; in such condition ~2.1 HS disaccharides are available on average per BMP-2 dimer. A small non-specific

binding of BMP-2 to the SAv monolayer has to be considered when high BMP-2 concentrations are used (**Figure S4A**). At high concentration it is also possible that several BMP-2 molecules interact with each other forming aggregates (**Figure S4B**). Moreover, BMP-2 in solution has been found to have a limited physical stability, with aggregates of various sizes forming in a pH-dependent manner.[30] Future studies using shorter oligosaccharides (down to 3 disaccharides) would be useful to study the minimal HS/Hp disaccharides length able to bind BMP-2.

The desorption of BMP-2 upon buffer rinsing is well described by the exponential function (**Figure S3A**, red line):

$$\Gamma = \Gamma_r e^{-k_{off}\Delta t} + \Gamma_{ir} \quad (2)$$

with an apparent off-rate $k_{off} = 6.1 \pm 1.9 \times 10^{-4}\ s^{-1}$. Γ_{ir} and Γ_r correspond, respectively, to BMP-2 fractions that are irreversibly and reversibly bound to the b-HS film. The fit reveals similar values for Γ_{ir} and Γ_r, meaning that approximately 50% of BMP-2 is released from the b-HS film. The heterogeneous structure of HS chains[28] and the spectrum of binding sites and affinities that results from it may well explain the presence of a BMP-2 fraction that binds HS reversibly and another fraction that binds HS stably.

SE was also used to control the surface density of the active biomolecules, a fundamental piece of information to perform studies on BMP-mediated cellular responses (**Figure 2**). To this end, the assembly of biomimetic surfaces was followed step by step, as for the QCM-D measurements. The areal mass densities obtained from the SE data are reported in **Table 1**. b-HS binds to SAv (**Figure 2A** and **Table 1**) and, considering SAv molecular mass of 60 kDa, the amount of HS bound on average per available biotin-binding site (assuming that two of four sites engage in the immobilization to the surface) is 6 ± 1.6 kDa. This value is below the average HS molecular mass employed (12 kDa). As previously discussed[23], this discrepancy is likely to be due to the large size distribution of HS in solution, i.e. capture on SAv has selected the shorter chains in the initial HS sample.

Thanks to the quantification of surface densities afforded by SE, we estimate that, at 96 nM concentration, each BMP-2 dimer has approximately 20 kDa of HS, corresponding to roughly 36 disaccharides, available on average at signal stabilization.

Noggin, does not bind to SAv (**Figure S5A**), as expected, but has a HS/Hp binding site[31] and indeed readily binds to the native b-HS film, at an areal mass density of ~ 112 ± 0.7 ng/cm^2 when incubated at ~200 nM (**Figure S5B**). When BMP-2 loaded b-HS film is incubated with noggin at the same concentration**,** noggin binds to the film (**Figure 2A** and **Table 1)**. The total amount of b-HS bound proteins (BMP-2 + noggin) is higher than the amount the individual proteins adsorbed on b-HS. This indicates that both proteins can be present in the b-HS film simultaneously, however it remains unclear whether b-HS-bound noggin recognizes at the same time BMP-2.

At a concentration of 96 nM, one b-BMP2 binds on average to two SAv molecules (**Figure 2B**), which is expected to be due to the larger dimensions of BMP-2 compared to SAv (~8 nm vs. ~5 nm). After immobilization of b-BMP-2 on SAv, we added noggin and observed that it binds at a ratio of 1 b-BMP2 to 0.7 noggin molecules (**Figure 2A**). As noggin is known to bind BMPs with a 1:1 stoichiometry,[17] this implies that ~30% of immobilized b-BMP2 is apparently not recognized by noggin. Plausible explanations are that the noggin binding site of some BMP-2 molecules is oriented towards the surface and therefore not accessible, and/or that the biotin-PEG-NHS is reacting with Lys 97 and/or Lys 101, thus protecting the binding epitope recognised by noggin[7] (**Figure 1A**). Noggin inhibits BMP signalling by blocking BMP binding epitopes for both BMPRI and BMPRII.[17] It is therefore likely that all b-BMP2 molecules recognized by noggin are also accessible to cell surface receptors.

To understand how the type of BMP-2 immobilization impacts on BMP-2 and noggin biological activity, we next performed functional experiments using BMP-responsive cells. Murine C2C12 myoblasts and mesenchymal stem cells from human bone marrow (hMSC)

were plated for short periods (30 to 180 minutes) on the biomimetic platforms to compare the bioactivity of soluble BMP-2 (sBMP-2), immobilized b-BMP-2 and b-HS/BMP-2.

We first characterized the signaling response in C2C12 cells, which form myotubes upon reaching confluency by switching to low serum condition,[32] but in presence of BMP-2 their myogenic differentiation is inhibited resulting in transdifferentiation towards the osteogenic lineage.[33] The phosphorylation level of SMAD 1/5 proteins, which are direct downstream effectors of the canonical BMP-SMAD signaling pathway, was used as indicator for BMP-2 bioactivity. We previously demonstrated that the covalent immobilization of BMP-2 on a surface *via* a heterobifunctional chemical linker retained the growth factor's biological activity and triggered BMP-mediated signaling in C2C12 cells.[34] In the present study, we investigate the effect of BMP-2 surface presentation *via* b-HS, which resembles its presentation in the ECM, in comparison to its surface immobilization *via* biotin. In both platforms BMP-2 surface concentration was determined to be in the range of 35 to 50 ng/cm^2 (**Table 1**). As reference, we used sBMP-2 at a concentration of 20 nM.[2] Surfaces presenting only b-HS were used as negative control. p-SMAD 1/5 phosphorylation kinetics were determined at 30, 90 and 180 minutes after cell plating (**Figure 3A and C**). While SMAD 1/5 phosphorylation induced by sBMP-2 decreases during a 3-hour stimulation period, the same could not be observed when BMP-2 is bound to b-HS or in the case of b-BMP2 immobilized on SAv. In particular, for the latter, SMAD 1/5 phosphorylation peak is delayed at 90 minutes and remained stable also for 180 minutes, in line with what has been previously observed for covalently immobilized BMP-2.[34] After 180 minutes, the levels of phosphorylated SMAD 1/5 are significantly higher in cells exposed to BMP-2 bound to b-HS than in presence of sBMP-2. Interestingly, for all the measured time points, a significant enhancement of p-SMAD 1/5 levels is observed when BMP-2 is presented through b-HS in comparison to b-BMP-2 (**Figure 3A**). To discard the possibility that b-HS enhances SMAD phosphorylation independently of sBMP-2, we used the mutated form of BMP-2 unable to bind HS (EHBMP-

2) on b-HS platforms. In this setting SMAD 1/5 phosphorylation levels at 180 minutes were similar for both sBMP-2 and sEHBMP-2, and in the case of EHBMP-2 they were also not increased by the presence of b-HS (**Figure S6**), suggesting that the enhancement of BMP-2 bioactivity is due to the specific presentation of BMP-2 by b-HS. It is thus conceivable that b-HS presents BMP-2 in the correct orientation to the BMP receptor complex.

Taken together, these results show that both immobilization strategies (b-BMP2 and b-HS/BMP-2) prolong the biological activity of the growth factor in comparison to its presentation to cells when added in the culture media. On b-HS presenting surfaces, the retention of BMP-2 might be favored by the cross-linking of the b-HS film (**Figure S2**). We further demonstrate that the presentation *via* b-HS enhances BMP-mediated signaling in C2C12 cells in comparison to its direct immobilization on SAv. To test the role of b-HS as co-factor and to better elucidate the nature of the binding between b-HS and BMP-2, the affinity of the complex b-HS/BMP-2 to BMP receptors and the functional blocking of HSPGs should be addressed in future studies.

We observed a similar result in the kinetics of SMAD 1/5 phosphorylation in primary hMSCs in response to the same immobilization strategy (**Figure 3C**). Indeed, on b-BMP2, SMAD 1/5 phosphorylation is prolonged for 180 min, while it decreased over time in presence of sBMP-2. In contrast to C2C12 cells, the presence of b-HS does not enhance BMP-2 signaling in hMSCs in comparison to the presentation of BMP-2 immobilized on SAv, which generates also high and sustained levels of p-SMAD 1/5 expression. Furthermore, a short-time stimulation of hMSCs on b-HS/BMP-2 and b-BMP2 presenting surfaces is sufficient to promote osteogenic differentiation. Cells plated for 90 minutes on the biomimetic platforms in the presence of BMP-2, either immobilized or added to the cell media, and then re-plated for 24 days on untreated tissue culture plates, express alkaline phosphatase (ALP), a marker of osteogenic differentiation,[1] without and additional factors (**Figure S7**). The observed ALP expression in cells exposed to surfaces presenting b-HS and BMP-2 is significantly higher

than the expression in cells exposed to sBMP-2. We conclude that early events triggered by the presentation of BMP-2 via b-HS are sufficient to activate the SMAD1/5 downstream signaling, which induces hMSCs differentiation towards the osteogenic lineage.

To assess whether the presence of b-HS prevents BMP-2 recognition by its antagonist noggin, as previously suggested for soluble HS (sHS),[20] we analyze short-term BMP-2 signaling on surfaces presenting BMP-2 bound to b-HS or b-BMP2 bound to SAv in the presence of a double molar excess of noggin in solution (**Figure 3B** and **D)**. As comparison, the same molar ratio has been used for sBMP-2 and for sBMP-2 bound to sHS. C2C12 and hMSCs responded in a comparable manner, demonstrating that noggin, by occupying to BMPRI and BMPRII binding epitopes, is able to inhibit the bioactivity of sBMP-2, sBMP-2 bound to sHS and b-BMP2 grafted on SAv. Surprisingly, when BMP-2 is bound to b-HS, the effect of noggin is negligible. To rule out the effect of BMP-2 released from b-HS (**Figure S3)** we exposed cells to an excess of soluble noggin, which we expect to antagonize the biological activity of the released BMP-2. We demonstrate that even in presence of an excess of noggin in solution (ref. b-HS BMP-2 noggin excess), Smad 1/5 phosphorylation levels remain high.

We speculate therefore that noggin does not efficiently recognize BMP-2 bound to b-HS, thus leaving a sufficient amount of BMP-2 which is bound to b-HS and still accessible to BMPRI and BMPRII to activate the SMAD 1/5 pathway. Future studies on the competition between b-HS/BMP-2 complex, noggin and BMP receptors might better clarify the impact of HS on BMP-2 interaction with noggin and with BMP receptors. Moreover, to consolidate our observations, platforms presenting controlled HS sulfation patterns and HS from different sources, are in the scope of future studies.

CONCLUSIONS:

We designed a biomimetic and versatile platform for molecular and cellular studies, which presents immobilized BMP-2 alone (b-BMP2) or bound to b-HS grafted *via* its reducing end

to SAv monolayers, similar to BMP-2 presentation by HSPGs in the ECM. By controlling the surface density and the stoichiometry of all components, we defined the apparent binding affinity between BMP-2 and b-HS and we demonstrated that BMP-2 can cross-link b-HS chains likely due to several independent Hp/HS binding sites at the N-terminus. These platforms represent therefore a versatile and tuneable biomimetic tool able to be exploited as active substrates for C2C12 and hMSCs stimulation towards osteogenic differentiation. We show that (i) surface immobilization of BMP-2 prolongs the p-SMAD 1/5 signalling activation with respect to the soluble BMP-2, (ii) the specific presentation *via* b-HS enhances the p-SMAD 1/5 levels on C2C12 cells and prevents the antagonistic effect of noggin on both C2C12 and hMSCs. Our study, therefore, highlights the potential importance of ECM HSPGs as regulators of BMP-2 activity, giving new insights into the molecular basis of ECM-BMP interactions and opening avenues for novel strategies to design biomimetic materials functionalized with BMP-2 in regenerative medicine.

Experimental Section

Further information on the experimental materials and methods are available in the supporting information.

Supporting Information

Supporting Information is available from the Wiley Online Library.

Acknowledgements

We thank Prof. Joachim Spatz (Dept. Biophysical Chemistry, Heidelberg University and Max Planck Institute for Medical Research, Heidelberg) for his kind support and fruitful discussions, Dr. Hugues Lortat-Jacob (IBS, Grenoble, France) for providing HS and valuable feedback on the experiments; Prof. Walter Sebald, (Würzburg University, Germany) for providing EHBMP-2. Aïseta Baradji (University of Liverpool, UK and CICbiomaGUNE, San

Sebastian, Spain) for helping with the SUV preparation; Dr. Burcu Minsky (Max Planck Institute for Intelligent Systems, Stuttgart) for support on SE measurements and, *of course,* the Cell Adhesion and Signalling group (Heidelberg University). This project has received funding from: European Union's Framework Program for Research and Innovation Horizon 2020 (2014-2020) under the Marie Sklodowska-Curie Grant Agreement No. 658334 H2020-MSCA-IF-2014 and from CellNetworks Cluster, Heidelberg University, under the CellNetworks Postdoctoral Program 2014-2015. EACA greatly acknowledges the support of DFG (SFB TRR 79 projects M9 and B5). EM, SW, JPS and EACA thank the Max Planck Society for support. RPR acknowledges the Spanish Ministry for economy and competitiveness (project MAT2014-54867-R). PK has received funding from DFG Forschergruppe FOG 2165. PK and CH greatly acknowledge support by BSRT Berlin School for Regenerative Therapies".

Received: ((will be filled in by the editorial staff))
Revised: ((will be filled in by the editorial staff))
Published online: ((will be filled in by the editorial staff))

Reference:

[1] H. M. Ryoo, M. H. Lee, Y. J. Kim, *Gene*. **2006**. *366*, 51.

[2] T. Katagiri, A. Yamaguchi, M. Komaki, E. Abe, N. Takahashi, T. Ikeda, V. Rosen, J. M. Wozney, A. Fujisawa-Sehara, T. Suda, *J Cell Biol*. **1994**. *127*, 1755.

[3] A. Asakura, M. Komaki, M. Rudnicki, *Differentiation*. **2001**. *68*, 245.

[4] F. Liu, A. Hata, J. C. Baker, J. Doody, J. Carcamo, R. M. Harland, J. Massague, *Nature*. **1996**. *381*, 620.

[5] M. Geiger, R. H. Li, W. Friess, *Adv Drug Deliv Rev*. **2003**. *55*, 1613.

[6] B. Sedaghati, B. Hoyer, A. Aigner, M.C. Hacker, M. Schulz-Siegmund, *Regenerative Medicine - from Protocol to Patient: 3. Tissue Engineering, Biomaterial and Nanotechnology*, Vol. 3, Springer, **2016**.

[7] S. Ahmed, R. P. Metpally, S. Sangadala, B. V. Reddy, *J Mol Graph Model*. **2010**. *28*, 670.

[8] E. Migliorini, A. Valat, C. Picart, E. A. Cavalcanti-Adam, *Cytokine Growth Factor Rev*. **2016**. *27*, 43.

[9] M. M. Martino, J. A. Hubbell, *Faseb j*. **2010**. *24*, 4711.

[10] X. Jiao, P. C. Billings, M. P. O'Connell, F. S. Kaplan, E. M. Shore, D. L. Glaser, *J Biol Chem*. **2007**. *282*, 1080.

[11] D. S. Bramono, S. Murali, B. Rai, L. Ling, W. T. Poh, Z. X. Lim, G. S. Stein, V. Nurcombe, A. J. van Wijnen, S. M. Cool, *Bone*. **2012**. *50*, 954.

[12] R. Ruppert, E. Hoffmann, W. Sebald, *Eur J Biochem*. **1996**. *237*, 295.

[13] I. Matsuo, C. Kimura-Yoshida, *Philos Trans R Soc Lond B Biol Sci*. **2014**. *369*.

[14] M. C. Fisher, Y. Li, M. R. Seghatoleslami, C. N. Dealy, R. A. Kosher, *Matrix Biol*. **2006**. *25*, 27; J. Huegel, M. Enomoto-Iwamoto, F. Sgariglia, E. Koyama, M. Pacifici, *Am J Pathol*. **2015**. *185*, 1676.

[15] W. J. Kuo, M. A. Digman, A. D. Lander, *Mol Biol Cell*. **2010**. *21*, 4028.

[16] B. L. Viviano, S. Paine-Saunders, N. Gasiunas, J. Gallagher, S. Saunders, *J Biol Chem*. **2004**. *279*, 5604.

[17] J. Groppe, J. Greenwald, E. Wiater, J. Rodriguez-Leon, A. N. Economides, W. Kwiatkowski, M. Affolter, W. W. Vale, J. C. Izpisua Belmonte, S. Choe, *Nature*. **2002**. *420*, 636.

[18] G. Sanchez-Duffhues, C. Hiepen, P. Knaus, P. Ten Dijke, *Bone*. **2015**. *80*, 43; Y. Matsumoto, K. Matsumoto, F. Irie, J. Fukushi, W. B. Stallcup, Y. Yamaguchi, *J Biol Chem*. **2010**. *285*, 19227.

[19] R. Gomes, C. Kirn-Safran, M. C. Farach-Carson, D. D. Carson, *J Musculoskelet Neuronal Interact*. **2002**. *2*, 511.

[20] S. Murali, B. Rai, C. Dombrowski, J. L. Lee, Z. X. Lim, D. S. Bramono, L. Ling, T. Bell, S. Hinkley, S. S. Nathan, J. H. Hui, H. K. Wong, V. Nurcombe, S. M. Cool, *Biomaterials*. **2013**. *34*, 5594.

[21] S. Sarrazin, W. C. Lamanna, J. D. Esko, *Cold Spring Harb Perspect Biol*. **2011**. *3*.

[22] D. Thakar, E. Migliorini, L. Coche-Guerente, R. Sadir, H. Lortat-Jacob, D. Boturyn, O. Renaudet, P. Labbe, R. P. Richter, *Chem Commun*. **2014**. *50*, 15148.

[23] E. Migliorini, D. Thakar, R. Sadir, T. Pleiner, F. Baleux, H. Lortat-Jacob, L. Coche-Guerente, R. P. Richter, *Biomaterials*. **2014**. *35*, 8903.

[24] W. A. Hendrickson, A. Pahler, J. L. Smith, Y. Satow, E. A. Merritt, R. P. Phizackerley, *Proc Natl Acad Sci U S A*. **1989**. *86*, 2190.

[25] N. S. Gandhi, R. L. Mancera, *Biochim Biophys Acta*. **2012**. *1824*, 1374.

[26] E. Migliorini, D. Thakar, J. Kuhnle, R. Sadir, D. P. Dyer, Y. Li, C. Sun, B. F. Volkman, T. M. Handel, L. Coche-Guerente, D. G. Fernig, H. Lortat-Jacob, R. P. Richter, *Open Biol*. **2015**. *5*.

[27] J. T. Gallagher, J. E. Turnbull, M. Lyon, *Int J Biochem*. **1992**. *24*, 553.

[28] C. I. Gama, S. E. Tully, N. Sotogaku, P. M. Clark, M. Rawat, N. Vaidehi, W. A. Goddard, 3rd, A. Nishi, L. C. Hsieh-Wilson, *Nat Chem Biol*. **2006**. *2*, 467.

[29] N. Jastrebova, M. Vanwildemeersch, U. Lindahl, D. Spillmann, *J Biol Chem*. **2010**. *285*, 26842; M. Maccarana, Y. Sakura, A. Tawada, K. Yoshida, U. Lindahl, *J Biol Chem*. **1996**. *271*, 17804.

[30] L. Luca, M. A. Capelle, G. Machaidze, T. Arvinte, O. Jordan, R. Gurny, *Int J Pharm*. **2010**. *391*, 48.

[31] S. Masuda, K. Namba, H. Mutai, S. Usui, Y. Miyanaga, H. Kaneko, T. Matsunaga, *Biochem Biophys Res Commun*. **2014**. *447*, 496.

[32] D. Yaffe, O. Saxel, *Nature*. **1977**. *270*, 725.

[33] T. Katagiri, S. Akiyama, M. Namiki, M. Komaki, A. Yamaguchi, V. Rosen, J. M. Wozney, A. Fujisawa-Sehara, T. Suda, *Exp Cell Res*. **1997**. *230*, 342.

[34] E. H. Schwab, T. L. Pohl, T. Haraszti, G. K. Schwaerzer, C. Hiepen, J. P. Spatz, P. Knaus, E. A. Cavalcanti-Adam, *Nano Lett*. **2015**. *15*, 1526.

[35] T. L. Pohl, J. H. Boergermann, G. K. Schwaerzer, P. Knaus, E. A. Cavalcanti-Adam, *Acta Biomater*. **2012**. *8*, 772; P. Paarmann, G. Dorpholz, J. Fiebig, A. R. Amsalem, M. Ehrlich, Y. I. Henis, T. Muller, P. Knaus, *Int J Biochem Cell Biol*. **2016**. *76*, 51; T. Takada, T. Katagiri, M. Ifuku, N. Morimura, M. Kobayashi, K. Hasegawa, A. Ogamo, R. Kamijo, *J Biol Chem*. **2003**. *278*, 43229.

[36] B. Mulloy, C. Gee, S. F. Wheeler, R. Wait, E. Gray, T. W. Barrowcliffe, *Thromb Haemost*. **1997**. *77*, 668.

[37] R. Richter, A. Mukhopadhyay, A. Brisson, *Biophys J*. **2003**. *85*, 3035.

[38] N. B. Eisele, S. Frey, J. Piehler, D. Gorlich, R. P. Richter, *EMBO Rep*. **2010**. *11*, 366.

[39] I. Carton, A. R. Brisson, R. P. Richter, *Anal Chem*. **2010**. *82*, 9275.

[40] G. V. Dubacheva, T. Curk, B. M. Mognetti, R. Auzely-Velty, D. Frenkel, R. P. Richter, *J Am Chem Soc*. **2014**. *136*, 1722.

[41] M. B. Huglin, *Journal of Applied Polymer Science*. **1965**. *9*, 1097.

[42] R. P. Richter, K. B. Rodenhausen, E. N. B.;, M. Schubert, *Coupling Spectroscopic Ellipsometry and Quartz Crystal Microbalance to Study Organic Films at the Solid-Liquid Interface*, Vol. 52, Springer, Heidelberg **2014**.

[43] V. Hagel, T. Haraszti, H. Boehm, *Biointerphases*. **2013**. *8*, 36; T. T. Tsay, K. A. Jacobson, *Biophys J*. **1991**. *60*, 360.

[44] W. Wagner, P. Horn, M. Castoldi, A. Diehlmann, S. Bork, R. Saffrich, V. Benes, J. Blake, S. Pfister, V. Eckstein, A. D. Ho, *PLoS One*. **2008**. *3*, e2213.

[45] J. Kopf, P. Paarmann, C. Hiepen, D. Horbelt, P. Knaus, *Biofactors*. **2014**. *40*, 171.

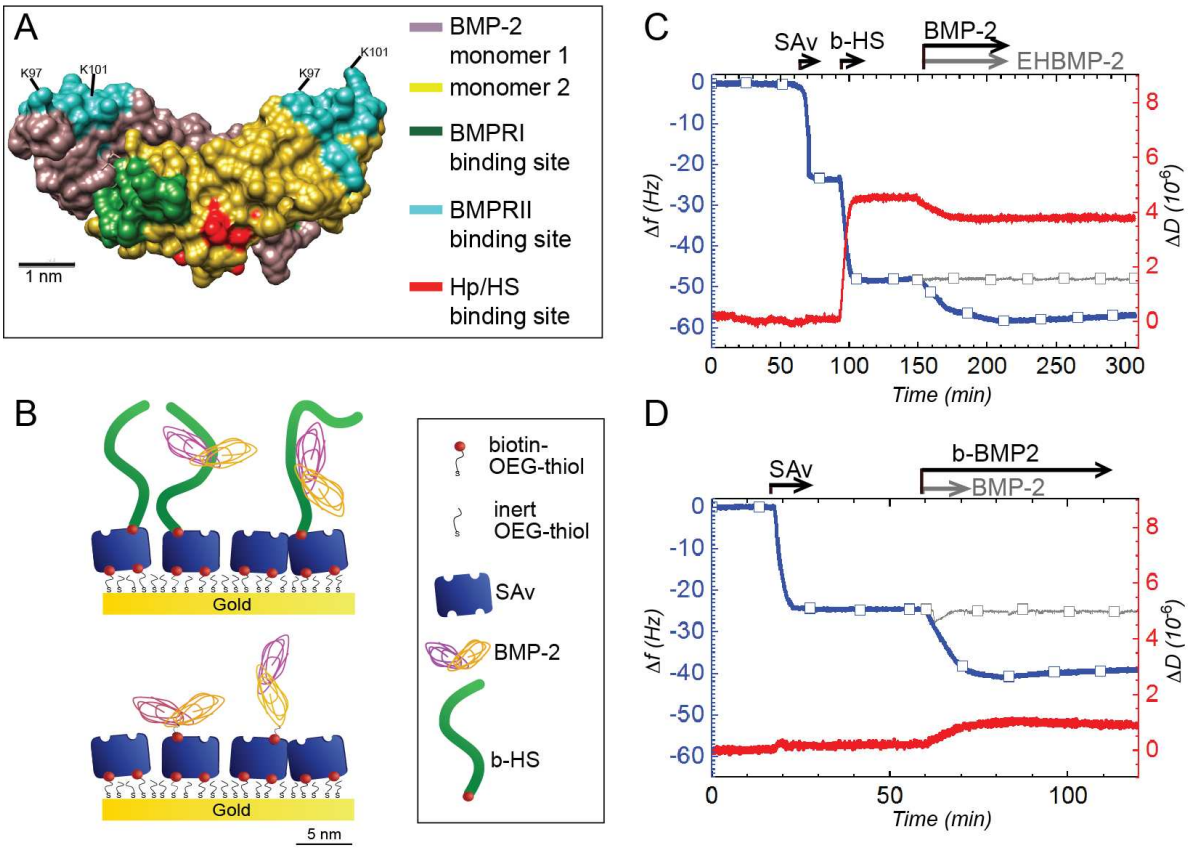

Figure 1. A: BMP-2 homodimer structure (PDB: 3BMP). **B**: Schematic representation of the biomimetic platforms. **C-D**: QCM-D characterization. Frequency shifts: Δf - *blue lines with square symbols*; dissipation shifts: ΔD - *red lines*. Start and duration of incubation steps are indicated by *arrows*; during all other times, the surface was exposed to working buffer.

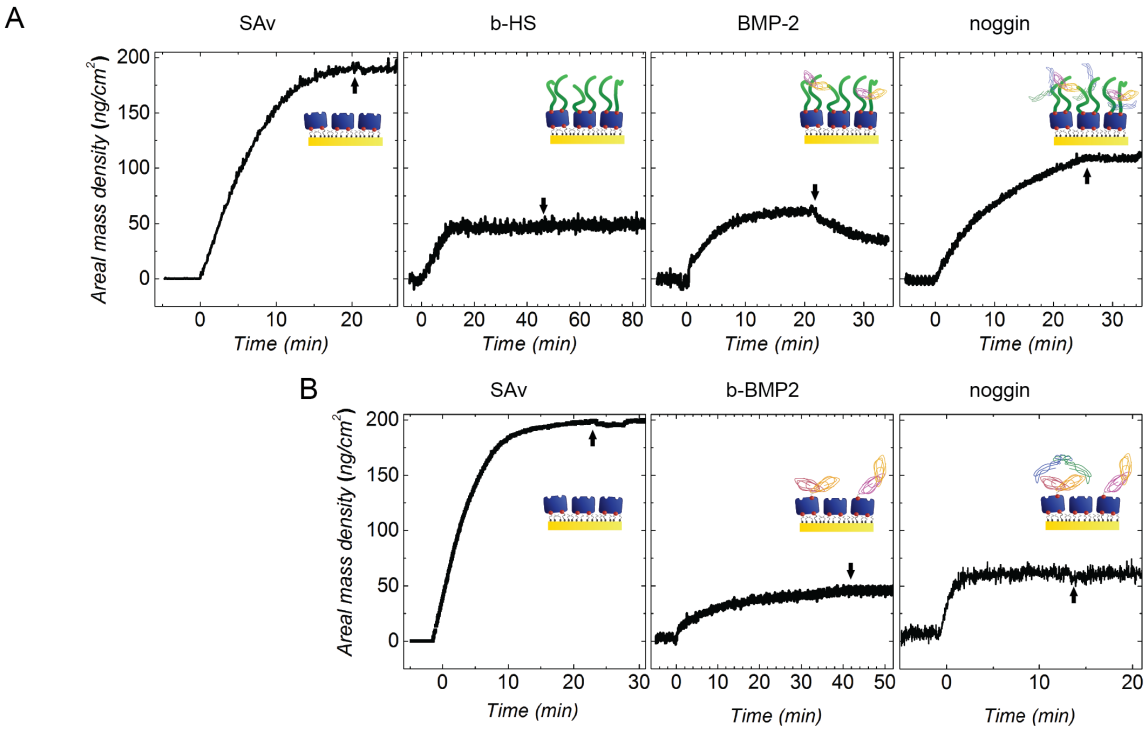

Figure 2. Surface functionalization is followed *in situ* by SE on a gold-supported OEG monolayer. Sample concentrations are: 83 nM SAv, 0.8 µM b-HS, 96 nM BMP-2, b-BMP2 and 200 nM noggin. Each incubation step started at 0 min; start of rinsing in working buffer is indicated by arrows.

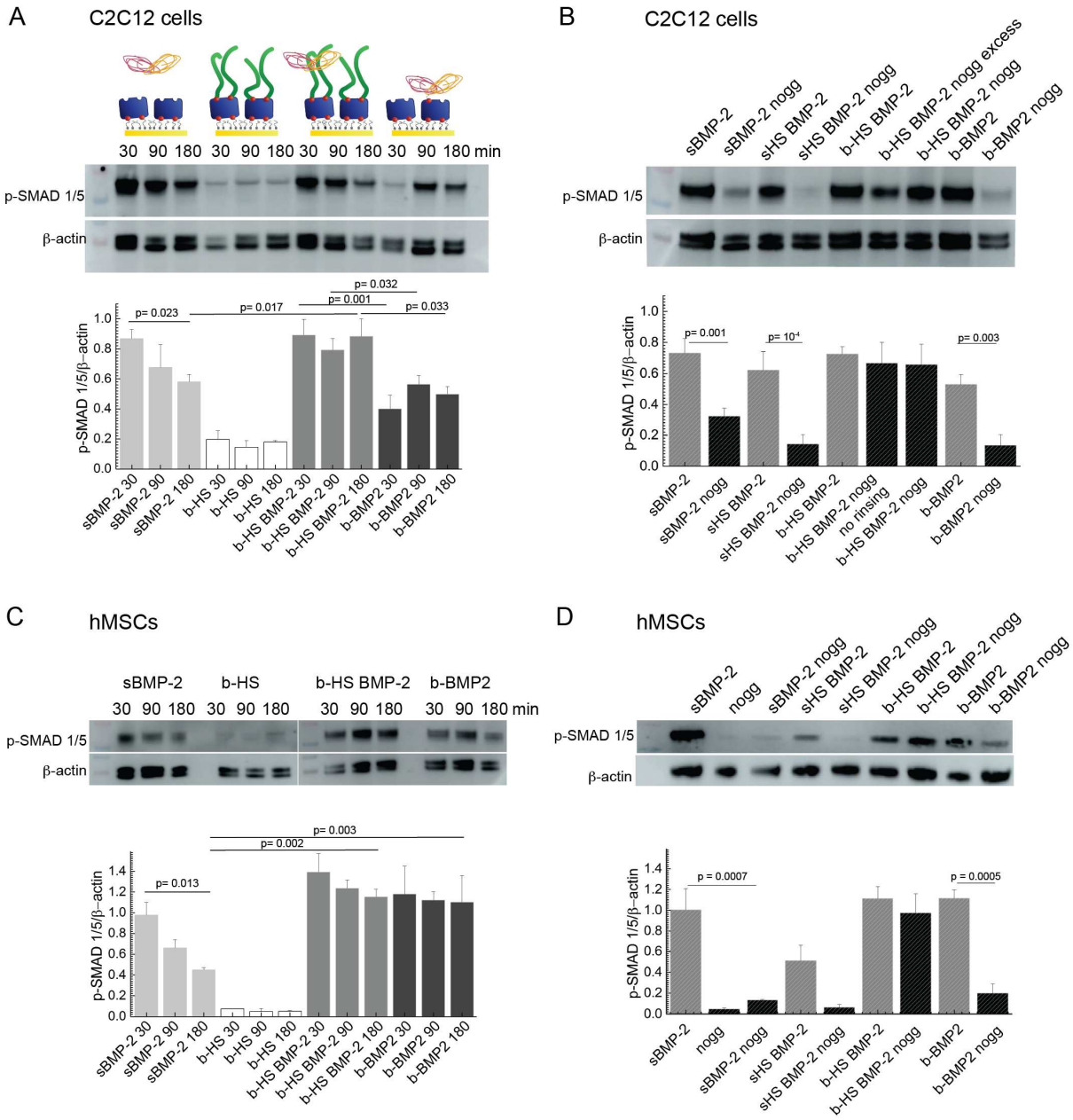

Figure 3. C2C12 cells (**A, B**) and hMSCs (**C, D**) plated on functionalized surfaces and lysed, at different time points (**A, C**) or after 90 minutes on substrates incubated with or without noggin (**B, D,**). p-SMAD 1/5 expression analyzed by Western Blot.

Table 1. Data was extracted from SE measurements at signal stabilization (**Figure 2**). Mean values and standard errors from the mean were derived from 3 independent measurements. On the basis of these numbers we quantify the number of molecules grafted per unit surface area and the stoichiometry of binding.

Compound	**Areal mass density (ng/cm^2)**
SAv	204.3±9.9

+ b-BMP2	44.2±4.6
+ noggin	57.6±2.1
b-HS	40.7±3.5
+ BMP-2 $_{(eq)}$	53.2±4.6
+ BMP-2 $_{(rins)}$	35.3±2.7
+ Noggin	112±4.1

$^{(eq)}$ value close to equilibrium during BMP-2 injection; $^{(rins)}$ value after BMP-2 rinsing with working buffer until plateau was reached.

Table of contents: Biomimetic platforms reproducing *in vitro* the BMP-2 presentation *via* extracellular matrix (ECM)-associated heparan sulfate proteoglycans. A bottom-up approach is used to functionalize biomimetic surfaces and to investigate the role of ECM-associated heparan sulfate on the biological activity of BMP-2.

Keyword: BMP-2, heparan sulfate, extracellular matrix, noggin, biomimetic platforms

Elisa Migliorini, Patrick Horn, Tamás Haraszti, Seraphine V. Wegner, Christian Hiepen, Petra Knaus, Ralf P. Richter and E. Ada Cavalcanti-Adam**

Title: Enhanced biological activity of BMP-2 bound to surface-grafted heparan sulfate

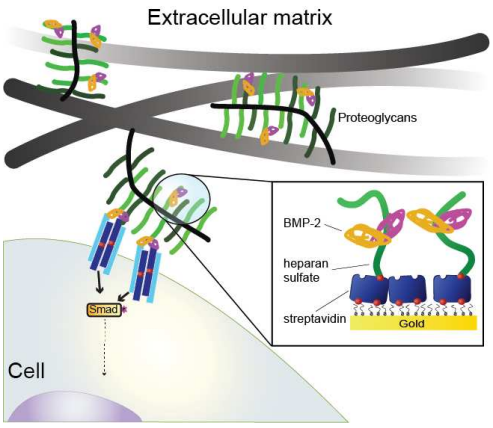

ADVANCED BIOSYSTEMS

Supporting Information

for *Adv. Biosys.*, DOI: 10.1002/adbi.201600041

Enhanced Biological Activity of BMP-2 Bound to Surface-Grafted Heparan Sulfate

Elisa Migliorini, Patrick Horn, Tamás Haraszti, Seraphine V. Wegner, Christian Hiepen, Petra Knaus, Ralf P. Richter, and Elisabetta Ada Cavalcanti-Adam**

Supporting Information

Title: Enhanced biological activity of BMP-2 bound to surface-grafted heparan sulfate

Elisa Migliorini, Patrick Horn, Tamás Haraszti, Seraphine V. Wegner, Christian Hiepen, Petra Knaus, Ralf P. Richter and E. Ada Cavalcanti-Adam**

Experimental Section:

Buffers, heparan sulfate and proteins

The working buffer used for surface functionalization and for all QCM-D, SE and FRAP measurements was made of Hepes (10 mM, Carl Roth GmbH, Karlsruhe, Germany), pH 7.4, and NaCl (150 mM, Sigma-Aldrich Chimie GmbH, Steinheim, Germany) in ultrapure water. $CaCl_2$ (2 mM, Sigma-Aldrich Chimie GmbH) was added to the working buffer to prepare lipid bilayers.

Heparan sulfate (HS) derived from porcine intestinal mucosa with an average molecular weight of 12 kDa and a polydispersity of 1.59 [36] (Celsus Laboratories, Cincinnati, OH, USA) was conjugated with biotin through an oligoethylene glycol (OEG) linker of approximately 1 nm length, site-specifically attached to the reducing end by oxime ligation.[22]

Human recombinant BMP-2 (26 kDa, homodimer), from a chinese hamster cell line, and human recombinant noggin (46 kDa, homodimer), from a mouse myeloma cell line, were purchased from R&D Systems Inc. (Minneapolis, MN, USA). BMP-2 was biotinylated by NHS-ester coupling using EZ-Link® NHS-PEG_{12}-Biotin 5.6 nm long (Thermo Scientific, Rockford, IL, USA). The coupling was performed at pH values between 8 and 8.5 for 1 h. Then the unbound EZ-Link® NHS-PEG_{12}-Biotin was removed by dialysis. BMP-2 with a substitution in the Hp/HS binding region (EHBMP-2)[12] was kindly provided by the group of Prof. Walter Sebald, University of Würzburg, Germany. Lyophilized streptavidin (SAv, 60 kDa) and fluorescently labeled SAv (fl-SAv; with atto565) were purchased from Sigma

Aldrich. All proteins were diluted to concentrations between 0.2 and 1 mg/mL in autoclaved working buffer and stored at -20°C. Thawed protein solutions were used within a week and further diluted as desired.

Sensors and surface preparation

QCM-D sensors with gold coating (QSX301) were purchased from Biolin Scientific (Västra Frölunda, Sweden). Glass cover slips (24×24 mm^2; Menzel Gläser, Braunschweig, Germany) were cleaned by immersion in freshly prepared piranha solution (i.e. a 1:3 (*v*/*v*) mixture of H_2O_2 (AppliChem GmbH, Darmstadt) and concentrated H_2SO_4 (Sigma Aldrich Chimie GmbH) for 1 h, rinsing with ultrapure water, and blow-drying with N_2. They were used as such or sputter-coated with a titanium adhesion layer (~1 nm and a semi-transparent gold film (~5 nm). All substrates were exposed to UV/ozone (BioForce, Ames, IA, USA) for 10 min prior to further use.

Functionalization of surfaces. Gold-coated surfaces were immersed overnight in ethanol solution (Carl Roth GmbH) of OEG thiol and biotinylated OEG thiol (Polypure, Oslo, Norway) at a total concentration of 1 mM and a molar ratio of 95:5, and subsequently immersed for 20 min in a solution of pure ethanol, and blow-dried in N_2.

Biotin-functionalized supported lipid bilayers (SLBs) were prepared by the method of vesicle spreading through exposure of small unilamellar vesicles (SUVs; at 50 μg/mL in working buffer supplemented with 2 mM $CaCl_2$) to glass surfaces, as described earlier.[37] SUVs were prepared by sonication, as described earlier[38], from mixtures of dioleoylphosphatidylcholine (DOPC) and dioleoylphosphatidylethanolamine-CAP-biotin (DOPE-CAP-b) (Avanti Polar Lipids, Alabaster, AL, USA) in a molar ratio of 95:5.

Assembly of biomimetic surface coatings

The step-by-step functionalization of the biomimetic surfaces is presented in **Figure 1**. Unless indicated otherwise, the following concentrations and exposure times were used: SAv – 370 nM, 20 min; b-HS – 830 nM, 20 min; BMP-2 and b-BMP2 – 96 nM, for 60 and 90 min respectively; noggin - 200 nM, 30 min. Under these conditions, we expect binding to saturate or equilibrate, irrespective of whether the solution is flown (in QCM-D and SE) or still (for cell assays).

Quartz crystal microbalance with dissipation monitoring (QCM-D)

With QCM-D, the shifts in resonance frequency (Δf, in Hz) and energy dissipation (ΔD, in dissipation units, 10^{-6}) of a quartz sensor crystal are measured as molecular binding events occur on the sensor surface. Δf relates to changes in the areal mass density (including hydrodynamically coupled solvent) of the biomolecular film, while ΔD reflects the film's mechanical properties. Measurements were performed with a Q-Sense E4 system equipped with 4 independent Flow Modules (Biolin Scientific). Sensors were coated with biotinylated OEG monolayers *ex situ* before the measurement. All other surface functionalization steps proceeded *in situ*. The system was operated in flow mode with a flow rate of typically 15 µL/min using a peristaltic pump (ISM935C, Ismatec, Zurich, Switzerland). The working temperature was 24°C. Δf and ΔD were measured at six overtones (i = 3, 5, ..., 13), corresponding to resonance frequencies of $f_i \approx$ 5, 15, 25, ..., 65 MHz; changes in dissipation and normalized frequency, $\Delta f = \Delta f_i/i$, of the fifth overtone (i = 5) are presented; any other overtone would have provided comparable information.

Spectroscopic ellipsometry (SE)

SE measures changes in the polarization of light upon reflection at a planar surface. We employed SE *in situ* to quantify the surface density of adsorbed biomolecules in a time-resolved manner. The setup consisted of a M-2000V SE system (J. A. Woollam, Lincoln, NE,

USA) combined with a flow module for combined E1 QCM-D/SE measurements mounted on a Q-Sense E1 system (Biolin Scientific).[39] Gold-coated QCM-D sensors were functionalized *ex situ* with a biotinylated OEG monolayer, and all other surface functionalization steps proceeded *in situ*, analogous to the QCM-D measurements. Biomolecular samples were injected at high flow rate (up to 100 µl/min) for two minutes until the solution reaches the surfaces. Then the molecular adsorption was monitored in still solution until a stable signal was achieved.

Surface densities were quantified through fitting of the data to optical models, as described in detail elsewhere.[40] Briefly, the gold film on the QCM-D sensors with the OEG monolayer was treated as a single isotropic layer and fitted as a B-spline substrate, and the biomolecular film was treated as a Cauchy layer. Areal mass densities were determined through de Fejter's equation, using refractive index increments, dn/dc, of 0.132 cm^3/g for b-HS[41] and 0.18 cm^3/g for all proteins.[42]

Fluorescence recovery after photobleaching (FRAP)

FRAP measurements were performed with a confocal laser scanning microscope (LSM 880, Zeiss, Jena, Germany) using a laser at 561 nm wavelength, a plan-apochromat 63 × / 1.4 oil immersion objective and a completely opened pinhole (1 mm diameter). FRAP was performed to quantify the lateral mobility of b-HS bound to fluorescently labeled SAv (fl-SAv; label Atto 565) on biotinylated glass-supported lipid bilayers (SLBs). The glass coverslips were cleaned by piranha solution and activated with UV ozone for 10 minutes. Fl-SAv was incubated at a concentration of 18 nM for 20 minutes. This incubation time leads to an incomplete (~50%) fl-SAv monolayer. After acquiring 3 pre-bleach images, a circular region with 15 µm radius in the center of the imaged area was bleached through an exposure for ~20 seconds to high laser intensity. The fluorescent recovery due to the lateral diffusion of the bleached and unbleached fl-SAv was then monitored through acquisition of post-bleached

images over a period of 5 minutes. The images acquired using this protocol were than analyzed by a custom-made Python script.

FRAP analysis was based on the diffusion equation in the spatial Fourier domain.[43] Background corrected intensities were normalized to compensate for bleaching caused by the imaging using the intensity of a not-bleached area at the edge of each frame.

$$I_{rel} = \frac{I - I_{bg}}{I_0 - I_{bg}} \frac{I_{ref\,0}}{I_{ref}} \tag{S1}$$

Where I_{rel} stands for the relative intensity of a given point in the image, I_{bg} is the background count (dark current) subtracted, and I_{ref} is the average reference intensity in the non-bleached area mentioned above.

Then, an inverse relative intensity profile ($1 - I_{\mathrm{rel}}$) was calculated, where we utilized the fact that $1 - c/c_0$ obeys the same diffusion law as $c(t,x,y)$, if the initial concentration $c_0(x,y)$ is constant (homogeneous sample). In Fourier space, denoting the spatial wave vector as q_i ($i = x,y$). we used the diffusion equation as:

$$c(q_x, q_y, t) = c_0(q_x, q_y)\exp(-4\pi^2(q_x^2 + q_y^2)Dt) \tag{S2}$$

We wrote an algorithm (provided in appendix 1) for this analysis allowing for extracting time dependent bleaching data at discrete wave vectors, which were then merged into one curve using the scaling with $4\pi^2q^2t$ as the abscissa, and including an additive constant (a_0) for the immobile fraction. Each curve was fitted individually, and then in merged form. This way we could discard experiments where spatial anisotropy was present (e.g. in the illumination). In order to stabilize the nonlinear fits, the data was weighted such, that the first 10% of the data points had a weight of 2 and the last 20% a weight of 6. Immobile fraction was determined as $a_0/(a_0+c_0)$ from the fits.

Cell cultures:

Mouse C2C12 myoblasts (ATCC CRL-1772) and mesenchymal stem cells from human primary material (hMSCs), are used for functional assays. C2C12 cells were cultured as sub-confluent monolayers in growth medium, consisting of Dulbecco's modified Eagle's medium (DMEM) (Gibco BRL) supplemented with heat inactivated fetal bovine serum (FBS, 10 %) (Sigma Aldrich) and penicillin/streptomycin (1 %, Gibco BRL) at 37 °C and 5 % CO_2 until passage number not superior to 12. hMSCs were isolated and cultured as described before.[44] Briefly, bone marrow from healthy donors for allogeneic transplantation was taken after written consent using guidelines approved by the Ethic Committee on the use of Human subjects at the Heidelberg University. After seeding of the mononuclear cell fraction evolving colonies were separated and hMSC further expanded in plastic culture flasks. Cells were cultured in a sub-confluent monolayer in growth medium consisting of DMEM-LG supplemented with MCDB201 (40% (v/v), Sigma), L–glutamine (2 mM, Sigma), penicillin/streptomycin (100 U/mL, Lonza), insulin transferrin selenium (1% (v/v), Sigma), linoleic acid albumin from bovine serum albumin (1% (v/v), Sigma), dexamethasone (10 nM, Sigma), L-ascorbic acid-2-phosphate (0.1 mM, Sigma), PDGF subunit B (PDGF-BB) and epidermal growth factor (EGF) (both 10 ng/mL; PreproTech, Rocky Hill, NJ, USA) and FCS (2% (v/v), HyClone, GE Healthcare). Medium was changed twice per week and early passages 3-5 were used in the experimental setups.

Protein isolation and western blot analysis:

After 4 hours of cellular starvation in serum-free media, approximately 10^5 cells are seeded on each biomimetic surface. To plate cells only on the functionalized surface area, we used pre-casted PDMS forms containing holes with the exact dimensions of the surfaces. In this way, the functionalized surfaces can perfectly fit on the PDMS forms and the total liquid amount is limited to 500 µL. Cells were stimulated with either 20 nM of soluble BMP-2 on SAv-coated surfaces or with immobilized BMP-2 on b-HS films or on SAv (b-BMP2) at a surface mass

density described in **Table 1**. Cells plated on b-HS films without any growth factor stimulation are considered as the negative control. To test the inhibitory effect of noggin, BMP-2 was first immobilized on the surfaces as described above and later noggin was added at a concentration of 200 nM for 1 hour. The excess of noggin is washed with working buffer except to the experiment shown in Figure 3B (ref b-HS BMP-2 noggin excess). To verify the differences induced by the GAG immobilization, we added the condition of soluble HS with and without noggin. Soluble HS (taken from the HS batch used for b-HS preparation) was first bound to BMP-2 by mixing HS (80 nM) and BMP-2 (20 nM) in Hepes buffer and 30 minutes after noggin (40 nM) was added. The same concentration of pre-mixed BMP-2/noggin complex in solution was used as control. Cells were plated on these surfaces and left for 90 minutes (**Figure 3B and D**).

EHBMP-2, which does not bind to b-HS (**Figure 1C**), was used at a concentration of 20 nM in solution. To verify the influence of b-HS, b-HS/EHBMP-2 platforms were not rinsed prior to cell seeding, to avoid the complete removal of the growth factor. Indeed, b-HS platforms incubated with EHBMP-2 (96 nM) and afterwards rinsed, did not promote SMAD 1/5 phosphorylation (data not shown).

After cell plating, culture medium was removed and cells were lysed with 100 µl of RIPA buffer (Sigma) containing anti-protease and anti-phosphatase inhibitors (Halt^{TM} Inhibitor cocktail 100X) and EDTA (0.5 M, both from Thermo Scientific).

Lysates were transferred into tubes and stored at -80°C. Protein extracts were separated by SDS-PAGE, transferred to nitrocellulose membrane and then probed with rabbit anti-p-SMAD 1/5 (1:1000, Cell Signaling Technology) and mouse anti-β-actin (1:2000 Sigma Aldrich) antibodies. Incubation with goat anti-rabbit or anti-mouse HRP-conjugated IgG (1:5000 Santa Cruz Biotechnology) was followed by detection with Amersham^{TM} ECL Prime Western Blotting Detection Reagent (GE Healthcare). ImageJ was used to determine the intensity of p-SMAD 1/5 and β-actin bands. All assays were repeated at least 4 times with

independent cell cultures. To evaluate the statistical significance between the samples, the ANOVA test with Fisher correction was applied, and a *p*-value for $\alpha = 0.05$ was extracted for each sample combination.

Alkaline phosphatase (ALP) staining:

hMSCs plated on the biomimetic platforms for 90 minutes, mechanically detached and re-plated at a concentration of $4 \times 10^3/cm^2$ on standard 48 well plates, were grown for 24 days in simple growing medium without growth factors. After this period hMSCs are fixed and the ALP expression tested with the Alkaline Phosphatase kit (Sigma-Aldrich).

Ilalastic 1.2.0 software is used to obtain a binary image (as shown in **Figure S7**) and Image J to calculate the percentage of the ALP positive areas on the image. Each sample has been entirely imaged with a 10× objective. Here, representative images are shown. $n = 30$ for each condition.

Statistical analysis:

All measurements were performed in at least three independent experiments. The means ± standard errors were calculated. Comparison of multiple groups was done by one-way analysis of variance (ANOVA). Statistical calculations were performed using OriginPro 2015 (OriginLab Corporation, MA, USA) and p-values are indicated in given figures with values of <0.05 being considered as statistically significant.

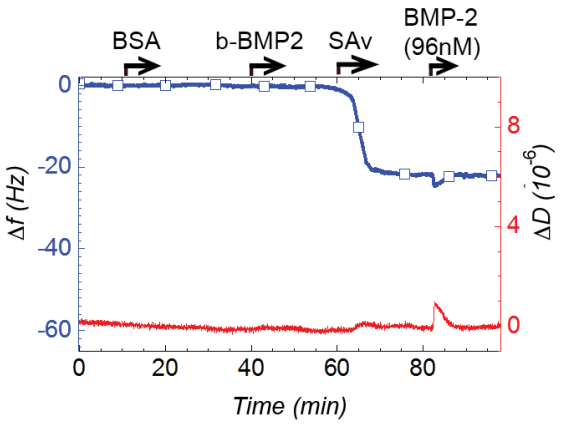

Figure S1: QCM-D characterization of the specificity of protein binding on the functionalized surfaces. Frequency shifts, Δf – *blue lines with square symbols*, dissipation shifts, ΔD – *red lines*. Start and duration of incubation steps with different samples are indicated by *arrows*; during all other times, the surface was exposed to working buffer. BSA 100 µg/mL does not bind to the OEG monolayer, on the contrary SAv can strongly bind forming a rigid monolayer. b-BMP2 and BMP-2 at a concentration of 96 nM are not adsorbing, respectively, to the OEG monolayer and to the SAv monolayer.

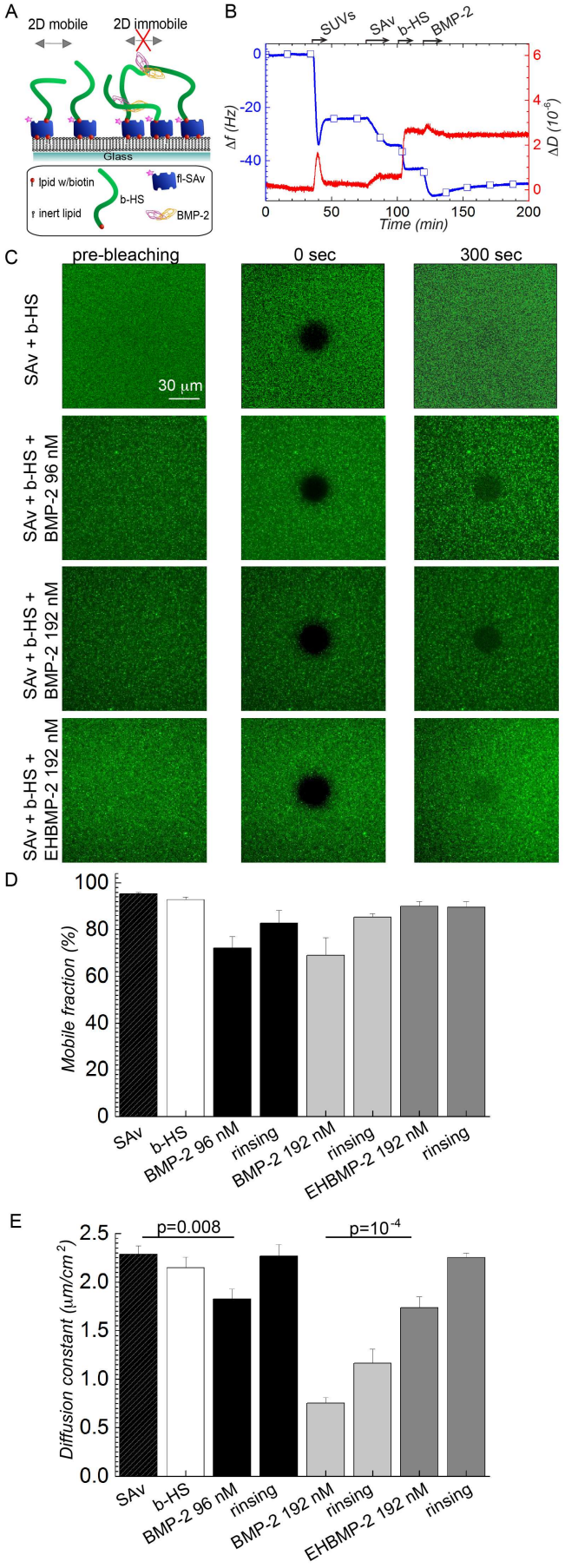
A
2D mobile
2D immobile
Glass
lpid w/biotin
inert lipid
fl-SAv
b-HS
BMP-2
B
SUVs
SAv
b-HS
BMP-2
Δf (Hz)
ΔD (10⁻⁶)
Time (min)
C
pre-bleaching
0 sec
300 sec
SAv + b-HS
30 μm
SAv + b-HS + BMP-2 96 nM
SAv + b-HS + BMP-2 192 nM
SAv + b-HS + EHBMP-2 192 nM
D
Mobile fraction (%)
SAv
b-HS
BMP-2 96 nM
rinsing
BMP-2 192 nM
rinsing
EHBMP-2 192 nM
rinsing
E
p=0.008
p=10⁻⁴
Diffusion constant (μm/cm²)
SAv
b-HS
BMP-2 96 nM
rinsing
BMP-2 192 nM
rinsing
EHBMP-2 192 nM
rinsing

Figure S2: HS film conformational changes upon BMP-2 binding. To verify if the increase in b-HS film rigidity upon BMP-2 binding (**Figure 1C**) is due to cross-linking of b-HS chains,[26] we implemented fluorescence recovery after photobleaching (FRAP), which provides information on the lateral diffusion of molecules. **A:** Scheme representing the platform used for FRAP experiments. We used silica-supported fluid lipid bilayers containing biotinylated lipids instead of gold-supported OEG monolayers as support, and fluorescently labelled SAv (SAv-Atto) for the attachment of b-HS and as a reporter for HS mobility. Cross-linking of two or more HS chains by BMP-2 dimers is expect to decrease HS mobility, whereas HS mobility should remain largely unchanged if each BMP-2 dimer binds only a single HS chain. **B**: QCM-D characterization of the surface functionalization. Frequency shifts, Δf – *blue lines with square symbols*, dissipation shifts, ΔD – *red lines*. Start and duration of incubation steps with different samples are indicated by *arrows*; during all other times, the surface was exposed to working buffer. SAv-Atto adsorption is interrupted after 20 minutes to avoid the formation of a dence monolayer thus permitting lateral mobility of the SAv molecules and the HS attached to it. BMP-2 at a concentration of 96 nM binds to the b-HS film and the dissipation shift slightly decreases.
C: Three pre-bleaching images were taken for each sample (one is shown in the first column) before the bleaching of the central area (first post-bleach image is shown in the second column). The recovery was recorded over 5 minutes after bleaching (last post-bleach image is shown in the third column). At least three independent measurements for each condition were performed. The images were analyzed by a custom-made python script to estimate the mobile fraction (**D**) and its diffusion constant (**E**). The mobile fraction and the diffusion constant of b-HS molecules decreased significantly after BMP-2 binding at a concentration of 192 nM (from 95% to 72%, and from 2.1 to 0.75 $\mu m^2/s$, respectively). At a lower concentration (96 nM), BMP-2 generates a lower but still significant reduction in HS diffusion. We used EHBMP-2, which does not bind to b-HS, indeed it does nor decrease the mobile fraction but just slightly reduced the diffusion constant (effect probably induced by molecular crowding). We conclude that BMP-2 might induce at lower concentration a transient cross-linking of the b-HS chains. The cross-linking stability improves at higher BMP-2 concentration. Overall, the effect on BMP-2 on b-HS film cross-linking, even if significant, is lower than other growth factors, as for example FGF-2,[26] which presents multiple distinct Hp/HS binding sites. We propose that, at increased BMP-2 concentration, more than one b-HS chain binds to each BMP-2 dimer, consistent with the presence of two or more independent Hp/HS binding sites at the BMP-2 dimer's N-terminus, which has previously been predicted.[25]
The function of HS film cross-linking remains to be determined, although it has been already shown that other (but not all) chemokines and growth factors crosslink HS films.[26] We hypothesize that simultaneous binding of BMP-2 to multiple HS chains *in vivo* helps the growth factor retention in the ECM. Moreover, the cross linking may also impact on matrix rigidity, thereby it could activate cell mechanical responses.[45]

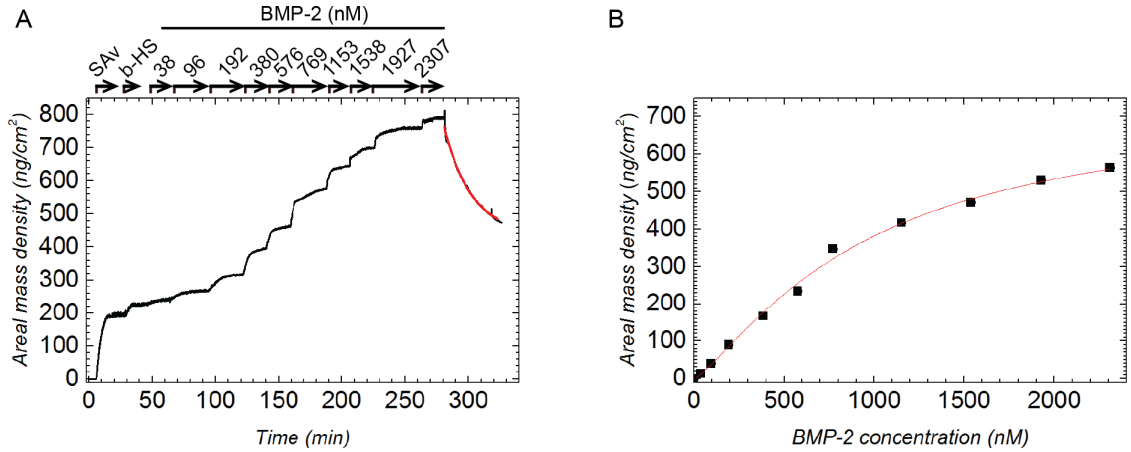

Figure S3: Quantification of the binding constant (K_d) and the off-rate (k_{off}) of the complex b-HS/BMP-2.
A: representative titration curve obtained by spectroscopic ellipsometry (SE) for the binding of BMP-2 to a film of b-HS grafted to a SAv monolayer. The start and duration of the incubation with different samples are indicated with arrows; during all other times, the surface was exposed to working buffer. Fits with the exponential **equation 2** to the desorption curves upon rinsing in buffer provide estimates for the off-rate constants $k_{off} = 6.1 \pm 1.9 \times 10^{-4}\ s^{-1}$. The values of the irreversibly (Γ_{ir}) and reversibly (Γ_r) bound BMP-2 fraction are respectively 428 and 392 ng/cm^2, meaning that approximately 50 % of BMP-2 is released from the b-HS film.
B: adsorbed amounts of BMP-2 close to equilibrium as a function of BMP-2 concentration in the solution phase, determined from A. The titration curve is modeled with a Langmuir isotherm (**equation 1**), with apparent K_d ~1.6 μM and Γ_{max} ~ 1000 ng/cm^2.

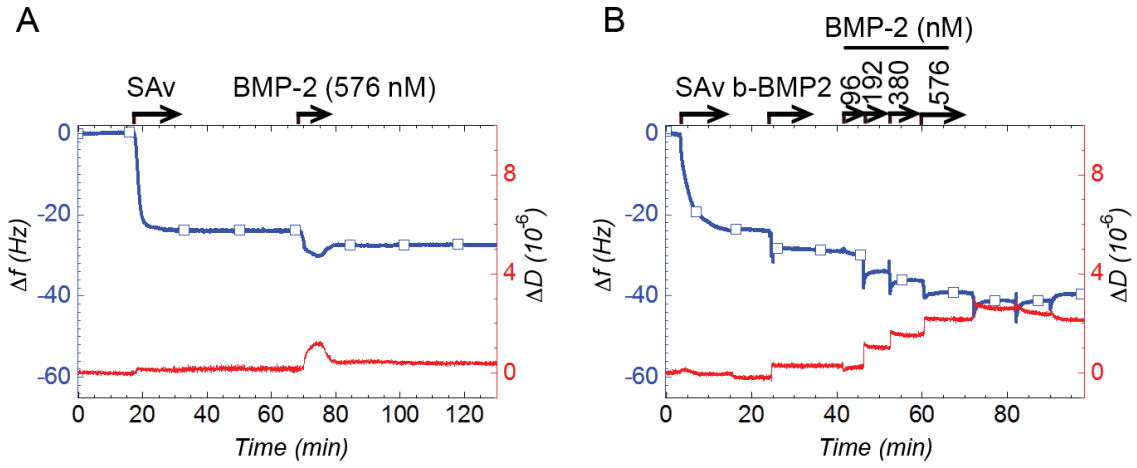

Figure S4: QCM-D characterization of the BMP-2 binding to SAv and to b-BMP2. Frequency shifts, Δf – *blue lines with square symbols*, dissipation shifts, ΔD – *red lines*. Start and duration of incubation steps with different samples are indicated by *arrows*; during all other times, the surface was exposed to working buffer. **A**: BMP-2 injected at high concentration (576 nM) generates a small non-specific binding to SAv monolayer. After rinsing the frequency shift is stabilized to approximately -3 ± 0.5 Hz. **B:** BMP-2 injected at increasing concentrations binds on b-BMP2 layer. BMP-2 is only partially released during consecutive rinsing steps. This observation suggests the formation of agglomerates at high protein concentration. For this measurement custom-made QCM-D Open Modules were used.

Protein injections and rinsing were performed from the top of the surface by exchanging the solution ten times.

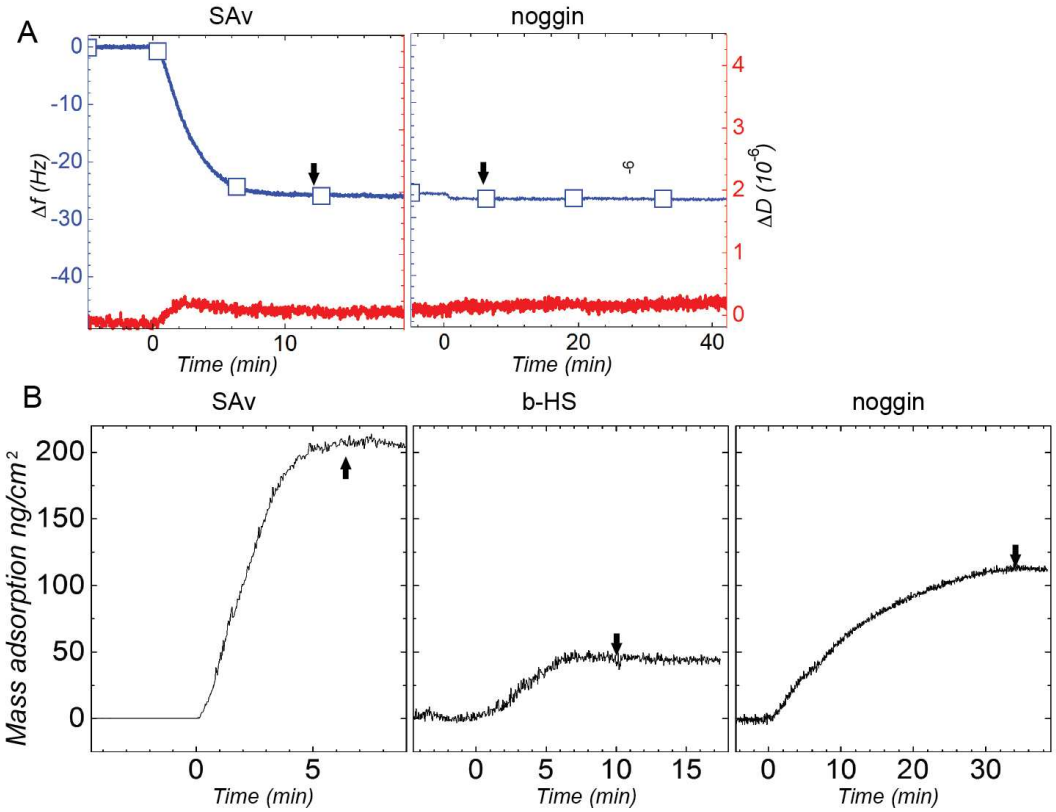

Figure S5: Noggin binding to the biomimetic platforms. The start of incubation steps is at 0 minutes, arrows indicate the rinsing with working buffer. **A:** QCM-D characterization of the noggin binding to SAv. Frequency shifts, Δf – *blue lines with square symbols*, dissipation shifts, ΔD – *red lines*. Noggin (200 nM) does not bind to SAv monolayer. **B**: Quantification by SE of the noggin surface density when injected at a concentration of 200 nM on a b-HS film.

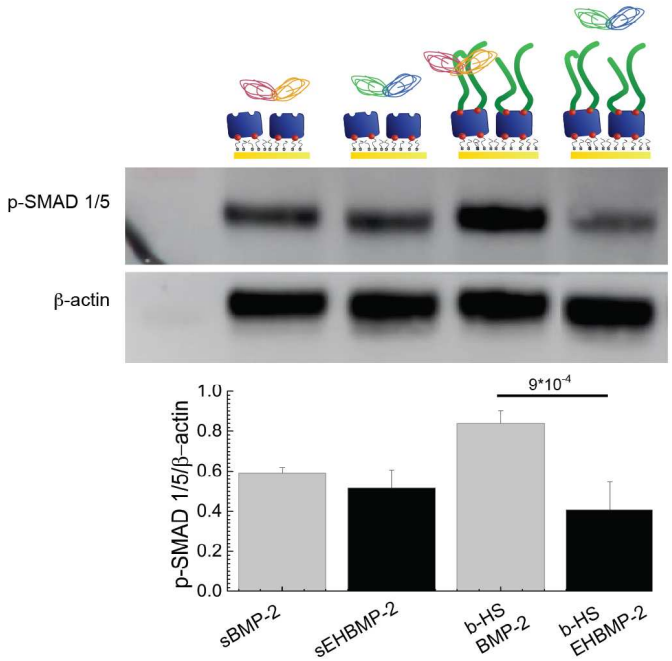

Figure S6: b-HS does not enhance the effect of EHBMP-2. C2C12 cells were plated on surfaces presenting the mutated BMP-2, with a heterologous sequence from human interleukin-2 at the place of the HS/Hp binding sites region, alone and combined with b-HS. After 180 minutes cells were lysed and the p-SMAD 1/5 levels followed with Western blotting analysis. Soluble EHBMP-2 induces the SMAD 1/5 phosphorylation in a comparable manner as BMP-2 at the same concentration (20 nM). The presence of b-HS with EHBMP-2 does not up-regulate the SMAD 1/5 phosphorylation as compared to soluble EHBMP-2 alone.

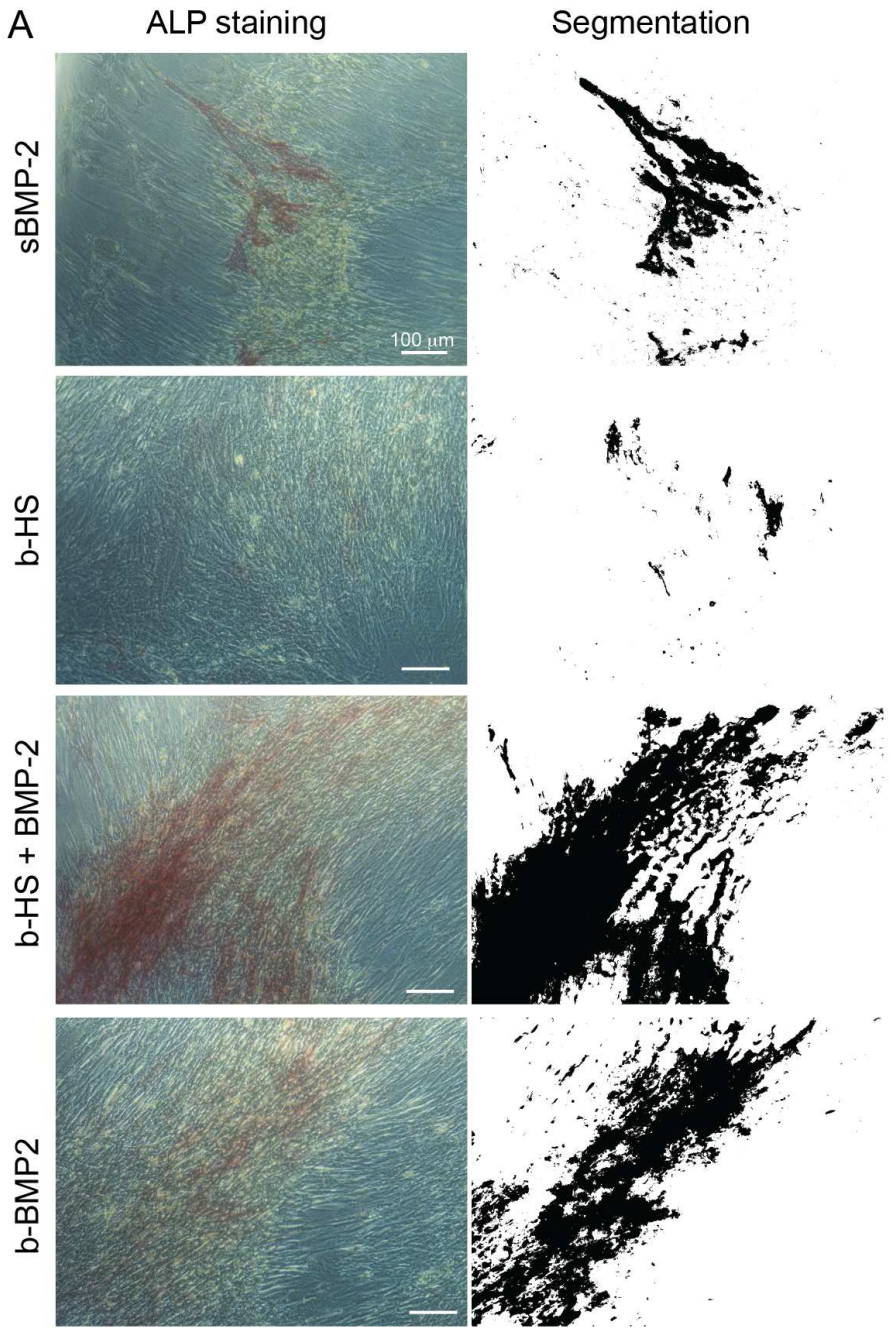
A
ALP staining
Segmentation
sBMP-2
b-HS
b-HS + BMP-2
b-BMP2
100 µm

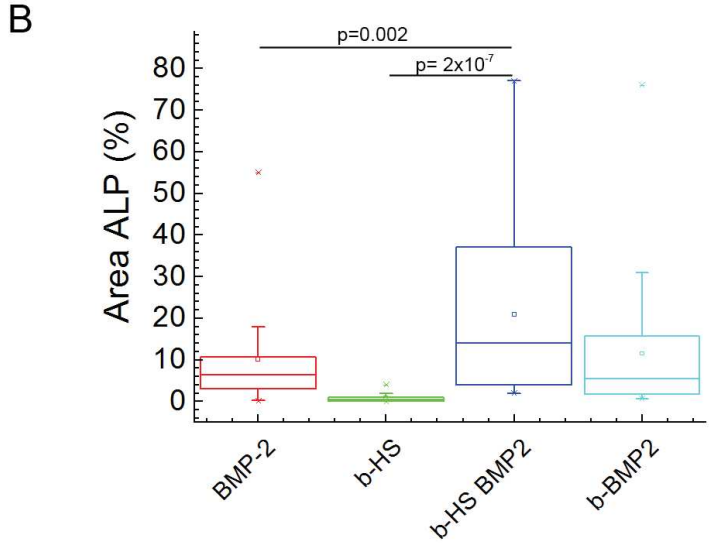
B
p=0.002
p= 2x10-7
Area ALP (%)
0
10
20
30
40
50
60
70
80
BMP-2
b-HS
b-HS BMP2
b-BMP2

Figure S7: Osteogenic differentiation of hMSCs induced by surfaces-presenting BMP-2. **A**: ALP histochemical assay performed 24 days after 90 minutes of hMSCs interaction with the biomimetic platforms presenting soluble and immobilized BMP-2. hMSCs were plated on normal coverslips successively the 90 minutes of stimulation, without adding osteogenic factors for the entire period of culture. The ALP expression after stimulation with b-HS has been used to evaluate the spontaneous differentiation without BMP-2 stimulation. Segmented images obtained with Ilastic software (right column) indicate the ALP positive regions of the original images (left column). **B**: quantification of the ALP positive areas as percentage of the total image area for each sample. Samples derived from b-HS BMP-2 surfaces presented a significantly higher ALP expression than sBMP-2.